HHS Public Access

Author manuscript

*Eur Neuropsychopharmacol*. Author manuscript; available in PMC 2021 November 01.

Published in final edited form as:

*Eur Neuropsychopharmacol*. 2020 November ; 40: 70–84. doi:10.1016/j.euroneuro.2020.06.004.

# Altered miRNA landscape of the anterior cingulate cortex is associated with potential loss of key neuronal functions in depressed brain

**Yoshino Yuta, M.D., Ph.D.**[1], **Bhaskar Roy, Ph.D.**[1], **Yogesh Dwivedi, Ph.D.**[*]

Department of Psychiatry and Behavioral Neurobiology, University of Alabama at Birmingham, Birmingham, Alabama, 35294, USA

## Abstract

MicroRNAs (miRNAs), a family of non-coding RNAs, have recently gained a considerable attention in neuropsychiatric disorders. Being a pleiotropic modulator of target gene(s), miRNA has been recognized as central to downstream gene regulatory networks. In the recent past, reports have suggested their role in changing the epigenetic landscape in brain of subjects with major depressive disorder (MDD). Anterior cingulate cortex (ACC) is a brain area implicated in several complex cognitive functions, such as impulse control, emotion, and decision-making and is associated with psychopathology associated with mood regulation. In this study, we examined whether MDD is associated with altered miRNA transcriptome in ACC and whether altered miRNA landscape is associated with modifications in specific gene network(s) at the functional level. Using next generation sequencing, it was observed that that 117 miRNAs (4.61%) were significantly upregulated and 54 (2.13%) were downregulated in MDD subjects (n=22) compared with non-psychiatric controls (n=25). Using 24 most significantly upregulated miRNAs in the MDD group, we determined functional enrichment of target genes and found them to be associated with long-term potentiation, neurotrophin signaling, and axon guidance. Intra- and inter-cluster similarities of enriched terms based on overrepresented gene list showed neurobiological functions associated with neuronal growth and survival. Web centric parameters and ontology enrichment functions identified two major domains related to phosphatidyl signaling, GTPase signaling, neuronal migration, and neurotrophin signaling. Our findings of altered miRNA

[*]Corresponding author: Yogesh Dwivedi, Ph.D., Elesabeth Ridgely Shook Professor, Director of Translational Research, UAB Mood Disorder Program, Co-Director, UAB Depression and Suicide Center, Department of Psychiatry and Behavioral Neurobiology, University of Alabama at Birmingham, SC711 Sparks Center, 1720 7th Avenue South, Birmingham, Alabama, USA, Phone: 01-205-975-8459, yogeshdwivedi@uabmc.edu.

[1]Equal contribution

Author contributions

YD conceptualized the idea. YY, BR analyzed the data. All the authors (YY, BR, YD) were involved in the preparation of the manuscript. They contributed to and approved the final manuscript.

Declaration of Competing Interest

Authors report no biomedical financial interests or potential conflicts of interest.

Supplementary materials

Supplementary material associated with this article can be found in the online version.

landscape along with a shift in targetome relate to previously reported morphometric changes and neuronal atrophy in ACC of MDD subjects.

**Keywords**

Anterior cingulate cortex; major depressive disorder; miRNA-seq; in-silico analysis; gene enrichment

## 1. Introduction

Major Depressive Disorder (MDD) is one of the debilitating mental disorders worldwide and the lifetime prevalence is 10.8% (Lim et al., 2018). Despite concerted efforts, the neurobiology of depression is not well understood, which is also reflected in the poor outcome of the current medication for MDD (Blackburn, 2019). Anterior cingulate cortex (ACC) is a brain area responsible for psychopathology associated with emotion regulation (Stevens et al., 2011). Neuroimaging and electrophysiological studies have strongly suggested the role of ACC in processing of emotional and sensory cues from various brain regions implicated in mood regulation (Pizzagalli et al., 2001; Wu et al., 2016). The critical role of ACC in mood regulation is further substantiated by the findings of significant changes in its morphology in MDD subjects (Drevets et al., 2008). Morphometric changes along with decreased gray matter volume in the subgenual region of ACC have been associated with both unipolar and bipolar depression (Wise et al., 2017). The largest worldwide study conducted by ENIGMA MDD Working Group detected gray matter loss in the orbitofrontal cortex, anterior and posterior cingulate, insula and temporal lobes (Schmaal et al., 2017). Additionally, smaller gray matter volume of ACC and bilateral insula have been reported in MDD subjects compared to bipolar subjects as well as healthy controls (Wise et al., 2017). Several rodent studies have also shown that gray matter reduction is strongly associated with dendritic atrophy and reductions of glia cells under the stressful condition (Radley et al., 2008; Wellman, 2001). The ACC has several functions such as attentional orienting, affective processing, and behavioral selection (Bush et al., 2000). As an integration center, ACC includes several important processing modules which help in controlling the cognitive and emotional network with afferent and efferent projections. Past studies have also suggested ACC related GABAergic deficiency in both adult and adolescent MDD brains (Gabbay et al., 2012; Price et al., 2009). Glutamatergic dysfunctionality has also been shown in ACC of adult MDD subjects (Cotter et al., 2002). These changes could be associated with altered gene functionality, as has previously been shown in other brain regions of MDD subjects (Malki et al., 2015; Roy et al., 2017b). A strong possibility of epigenetic regulation of aberrant gene expression cannot be ruled out given that environmental risk factors are critical in the complex behavioral outcomes associated with mood disorders (Wang et al., 2018). Moreover, several studies have examined MDD in the context of suicidal behavior and found to be driven by adverse environmental influence. It is important to mention that emotional turmoil in survivors of patients who died by suicide may last for a long time, and in some cases, may end with their own suicide. Thus, it is fundamental to understand the bereavement process after the suicide of a significant other in order to provide proper care, reduce stigma, and improve the outcomes. Although the role of

miRNAs is not well understood in the bereavement process or in their link to MDD leading to suicidal behavior (Pompili et al., 2013), postmortem brain studies provide critical information regarding completed suicide, which may help explain the molecular changes happening in the brain under such conditions. Recently, numerous studies have shown that non-coding RNAs, including microRNAs (miRNAs), can have significant epigenetic influence in the development of psychiatric disorders such as MDD (Briggs et al., 2015; Kocerha et al., 2015; Qureshi and Mehler, 2013; Roy et al., 2017a; Salta and De Strooper, 2012; Sartor et al., 2012). A recent qPCR-based study using a set of 29 miRNAs identified downregulation of two miRNAs (miR-184 and miR-34a) in the ACC of MDD subjects (Azevedo et al., 2016). However, the involvement of miRNA-mediated epigenetic regulation of altered ACC functions in MDD has not been evaluated in greater detail at transcriptome-wide level. In the present study, we examined transcriptome-wide differential regulation of miRNAs in a relatively large number of ACC samples from non-psychiatric controls (n=25) and MDD subjects (n=22) using miRNA-sequencing. Subsequently, the KEGG based pathway and gene ontology (GO) analysis were done based on predicted targets of top significantly altered miRNAs in the MDD group. The results helped us to comprehend the functional role of ACC-specific miRNA changes in MDD pathogenesis.

## 2. Experimental procedures

### 2.1. Subjects

The study was approved by the Institutional Review Board of the University of Alabama at Birmingham (UAB) under exemption 4. The study was performed in ACC obtained from the New South Wales Brain Tissue Resource Centre at the University of Sydney. ACC from a total of 25 non-psychiatric controls (hereafter referred as controls) and 22 MDD subjects were used. Detailed demographic and clinical characteristics of subjects are shown in Table 1. Demographic data included age, gender, race, postmortem interval (PMI), brain pH, cause of death, history of drug/alcohol abuse, and antidepressant toxicology at the time of death. There were no significant differences in age, PMI, brain pH between MDD and control subjects (Table 1). MDD group had 12 males and 10 females whereas control group had 15 males and 10 females. Within the MDD group, 10 subjects died by suicide and 12 died by causes other than suicide. Also, out of 22 MDD subjects, 4 had a history of alcohol abuse and 18 showed positive antidepressant toxicology at the time of death.

Detailed tissue dissection, preservation, quality control and detailed in earlier publications (Dedova et al., 2009; Sheedy et al., 2008). Briefly, the cerebrum, cerebellum and brainstem are divided in the sagittal plane. The cerebellar hemisphere and brainstem were removed from each cerebral hemisphere by transversely sectioning the brainstem through the rostral midbrain at the level of the superior colliculi. Each cerebral hemisphere and its contralateral cerebellar hemisphere and brainstem were assigned a “fresh” or “fixed” status on a random basis. The fresh hemisphere was cut into 1 cm coronal slices and several areas were dissected including ACC and digitally photographed. The tissue blocks and were frozen on precooled trays at a temperature of −80°C and were bagged into air-tight plastic bags. Detailed neuropathological examination was done for several brain regions. Blood samples taken at the time of autopsy were used for toxicology screens for therapeutic drugs.

toxicology including neuroleptics, paracetamol, and anti-depressants. Several assessments including, diagnostic characterization, review of agonal status, measurement of brain tissue pH, histological assessment of post-mortem autolysis and a full neuropathological to ensure the tissue integrity. Brain tissue pH was measured in cerebellar tissue (Harrison et al., 1995).

The post-mortem clinical diagnosis of each case was determined through extensive review of medical records by one of two independent clinicians. All psychiatric cases were confirmed by a psychiatrist retrospectively using the Diagnostic Instrument for Brain Studies – Revised (DIBS-R). The DIBS is semi-structured instrument designed specifically for postmortem psychiatric assessment using medical records and informants where available. This instrument is compliant with the Diagnostic and Statistical Manual of Mental Disorders. The DSMIV and DSMV Diagnostic Criteria were used in all psychiatric disorder cases.

### 2.2. Total RNA isolation from ACC

TRIzol ® (Invitrogen, Grand Island, NY, USA) was used to isolate RNA. The detail method has been described earlier (Roy et al., 2017a). The RNA purity was checked by Nanodrop (260/280 nm; cutoff ⩾ 1.8) and integrity by agarose gel electrophoresis. It was made sure that RNA Integrity Number (RIN) for all samples were within acceptable range of 7–8.

### 2.3. Library preparation and sequencing of miRNAs using total RNA from ACC

The isolated total RNA from ACC of all 47 subjects were sequenced using Genomic Core facility at University of Alabama at Birmingham following small RNA library preparation method. In brief, the RNA quality was checked on the Agilent BioAnalyzer for the presence of a strong 5S peak to assure the miRNA fraction. Total RNA was used in an initial ligation reaction to attach 3’ oligo with RNA ligase. A subsequent ligation was performed to add 5’ oligo, also with RNA Ligase. A primer specific for the 3’ oligo was used to generate 1st strand cDNA in a standard reaction. Double stranded cDNA was generated via PCR. The resulting library was checked for size and quality using the DNA High Sensitivity Chip on the Agilent BioAnalzyer. The libraries were quantitated via qPCR (KapaBiosystems), normalized to 3 nM, and loaded onto Illumina NextSeq 500 and sequenced with 75bp single end reads as per the manufacturer’s protocol. The miRNA profiling was conducted using Illumina NGS platform, libraries were created using Qiagen’s miRNA kit. The resulting libraries were standardized for concentration and sequenced on the NextSeq500 using 75 bp single end reads.

### 2.4. Analysis of miRNA sequencing data

Reads were trimmed, unique molecular identifier (UMI) sequences were identified and were aligned to miRbase and the human hg38 genome. Next, the count reads and UMIs were assigned to each miRNA. The UMIs were then normalized in Qiagen’s GeneGlobe Data Analysis Center (https://geneglobe.qiagen.com/us/analyze/). Based on normalized miRNA expression values across 25 control and 22 MDD subjects, the expression heat map was generated following a hierarchical clustering method. In the expression heat map, the miRNAs with high expression values are shown in green color and miRNAs with low expression values are shown in red (Fig. 1A). For the clustering purpose, the Euclidean method was used to measure the distance, and the average linkage algorithm was applied to

calculate the average pairwise distance between all pairs of points. To determine the miRNA expression changes in a biologically meaningful way, fold-change (FC) was calculated using the normalized miRNA expression in each test sample divided by the normalized miRNA expression in the control sample. For the geNorm and Total Molecular Tag Count normalization methods, the p values were calculated based on Student's t-test of the replicated normalized miRNA expression values for each miRNA in the control group and the MDD group. For the DESeq2 and Trimmed Mean of M (edgeR) normalization methods, the p values were determined by the respective Bioconductor software packages.

### 2.5. miRNA target gene prediction

GO analysis was done independently based on the predicted targets of miRNAs which were found to be significantly upregulated (FC≥ 2.0) in ACC of MDD subjects. To obtain a consensus list of predicted targets, in-silico prediction algorithm from eight different prediction programs (i.e., miRWalk, Microt4, miRanda, miRDB, Pictar2, PITA, RNA22, and Targetscan under miRWalk version 2.0 software package) was used. Next, a common list of targets that were shared by any five of them were used for further functional prediction analysis.

### 2.6. Prediction based pathway and GO analysis

The consensus list of predicted targets prepared from miRWalk (version 2.0) software was used to predict gene ontology (GO) terms using the ShinyGO program and KEGG (Kyoto Encyclopedia of Genes and Genomes) based pathway analysis using WEB-based GEne SeT AnaLysis Toolkit (WebGestalt, http://www.webgestalt.org/). The GO prediction analysis was done following an FDR corrected p-value cutoff 0.05 to determine the gene set enrichment in biological process (BP) and cellular component (CC) category separately. In BP, 30 most significant terms were used to plot the network with edge cutoff 0.05, whereas, in the CC, the connected nodes are presented with 40 most significant terms with edge cutoff 0.03. In each category, the enriched terms were used to create networks where nodes are presented with terms and connected with edges. If two nodes are connected, then they share 20% (default) or more genes. Bigger nodes represent larger gene sets. Thicker edges represent more overlapped genes. In WebGestalt, Over-Representation Analysis (ORA) with KEGG pathway was used to find the relevant pathways. Further, the gene list obtained from WebGestalt was filtered based on the parameters defining neurobiological functions associated with neuronal growth and survival. A short list of genes was further fed into Metascape program (http://metascape.org/gp/index.html#/main/step1) which uses 40 independent knowledge bases to integrate system level information and creates comprehensive gene list with designing features including gene annotation, pathway and functional enrichment. For creating the color-coded bar plot, the algorithm first identified all statistically enriched terms (Zhou et al., 2019). Next, accumulative hypergeometric p-values and enrichment factors were calculated and used for filtering them. Remaining significant terms were then hierarchically clustered into a tree based on Kappa-statistical similarities among their gene memberships. The tree was casted into terms using an optimized kappa threshold (0.3).

### 2.7. Statistical analysis

Statistical analyses were conducted using SPSS 25.0 software (IBM, Chicago, IL, USA). The Shapiro-Wilk test was used to assess the normality of the data. The average difference of age, PMI, and brain PH, was assessed by Student's t test. Differences in miRNA expression based on gender, alcohol abuse, antidepressants, and suicide were analyzed by Student's t test. Correlation between miRNA expression and age, brain pH, and PMI were evaluated by Pearson Product Moment analysis. Statistical significance was set at the 95% level ($p = 0.05$).

## 3. Results

### 3.1. MDD specific differential miRNA expression profile in ACC

From the differential expression analysis between control and MDD groups, a total of 2540 fully annotated miRNAs regardless of their statistical significance were detected. Using the normalized values of all miRNAs expressed across all 47 subjects, a hierarchically clustered expression heat map was generated (Fig. 1A) to show the differential expression profile between MDD and control subjects. Green and red color in the map show higher and lower expression values respectively. Following the average linkage clustering algorithm, the dendrogram was constructed to demonstrate the expression similarities. These miRNAs included both up and downregulated groups. Besides that, a set of 423 predicted (novel) miRNAs were also found to be altered in the MDD group. However, filtering the list of differentially regulated miRNAs following statistical significance ($p \leq 0.05$) resulted in the identification of a total 230 miRNAs including both annotated (171) and predicted (59) ones (Fig. 1B). For annotated miRNAs, 117 (4.61%) were upregulated and 54 (2.13%) were downregulated. From the list of 59 novel miRNAs, 50 miRNAs (11.8%) were found to be upregulated and 9 miRNAs (2.13%) were downregulated. In the significantly altered annotated miRNA group, sorting the list with ≥2 fold change (FC) value identified 24 highly upregulated miRNAs in the MDD group. Two separate tables have been presented to show all significantly ($p \leq 0.05$) altered miRNAs (Table 2). Topmost significantly expressed (*extremely upregulated*, FC cut off >2.0; and *downregulated*, FC cut off <0.5) miRNAs in the MDD group are highlighted with bold fonts in Table 2.

### 3.2. Effects of covariates toward extremely upregulated 24 miRNAs (fold change cut off >2.0)

The extremely upregulated 24 miRNAs were used for target prediction and gene ontology. These miRNAs were further evaluated for their association with covariates such as age, gender, brain pH, PMI, alcohol abuse, antidepressant toxicology, and suicide as cause of death. Detailed results are shown in the supplementary section (Table S1). None of the changes in miRNAs were associated with any of the covariates except age was negatively correlated with miR-4701–3p ($p=0.043$, $r=-0.407$) and brain pH was positively correlated with miR-6737–5p ($p=0.031$, $r=0.432$), miR-6075 ($p=0.040$, $r=0.423$), miR-4701–3p ($p=0.031$, $r=0.433$) in the control group. Within the MDD group, alcohol abuse had significant impact on the expression of miR-6077 ($p=0.012$), miR-6789–3p ($p=0.034$), miR-648 ($p=0.027$), and mir-4746–3p ($p=0.009$). There were no significant differences in

miRNA expression when MDD subjects who died by suicide were compared with those who died by causes other than suicide (Table S1).

### 3.3. Target gene prediction

Owing to the repressive nature of miRNAs in regulating target gene expression, top 24 significantly upregulated miRNAs (FC >2.0) were used for target gene prediction analysis following conservative prediction algorithm. As mentioned in methods section, a common list of targets that were shared by any five of the prediction algorithms was finalized. A total of 1092 predicted target genes were finally used for subsequent GO and KEGG based pathway analyses.

### 3.4. miRNA target gene-based gene ontology and pathway prediction

Following GO enrichment analysis with the predicted targets of significantly upregulated 24 miRNAs in ACC of MDD subjects, we found three separate clustering of GO terms under the BP category (p value cutoff <0.05 [FDR], Edge Cutoff: 0.3) (Fig. 2A). The clustered biological functions were plotted into networks to represent their relatedness. The nodes representing the GO terms are only connected through edges when they share 20% or more genes. The bigger nodes represent larger gene sets. Thicker edges represent more overlapped genes. Gross functional enrichments of genes for nucleic acid and protein metabolisms were identified as shown in the two left most clusters. The right most cluster in the network map demonstrates the presence of four enriched terms; all of which were central to neuronal growth and development (e.g., neurogenesis, nervous system development, neuron differentiation and generation of neurons). Next, another network map was created following the GO term enrichment under CC category (p value cutoff <0.05 [FDR], Edge Cutoff: 0.3) (Fig. 2B). The map showed predominant enrichment of terms correlated with somatic (neuronal cell body), somatodendritic and synaptic (pre, post synaptic, and synaptic vesicle) functions in central nervous system. Additionally, the targeted enrichment of genes was mapped translating to glutamatergic synapses which have earlier been suggested to be important in MDD associated ACC functions.

A pathway-based network map (p value cutoff <0.05 [FDR], Edge Cutoff: 0.2; most significant display terms: 50) was separately prepared showing the predicted involvement of various neuro-molecular pathways (Fig. 2C) earlier reported to be quite important in MDD pathogenesis. These include ErbB, Wnt, MAPK, mTOR, and phosphatidylinositol signaling. A significant enrichment of pathways related to immuno-inflammatory functions, mostly pro-inflammatory cytokines (IL-17 and TNF) and their regulating factors (NF-kappa B signaling) were also noted.

WebGestalt program was additionally used to further validate ShinyGO based findings based on putative targets of 24 significantly upregulated miRNAs. In both the KEGG pathway and GO analysis, top 10 pathways are listed according to significance level as a large number of pathways were hit (KEGG pathway, 271; BP, more than 2,000; CC, 779; molecular functions [MF], 1158) (Table 3 and 4). From the KEGG pathway, long-term potentiation (LTP, hsa04720) had the highest enrichment ratio (3.4). From the BP results, several GO terms were found that were primarily related to the central nervous systems (CNS) such as

neuron projection development (GO:0031175), neuron development (GO:0048666), generation of neurons (GO:0048699), neuron differentiation (GO:0030182), and neurogenesis (GO:0022008). From the CC results, CNS related GO terms such as synapse (GO:0045202), synapse part (GO:0044456), neuron part (GO:0097458), and neuron projection (GO:0043005) were found. In terms of MF, RNA polymerase II regulatory region DNA binding (GO:0001012) had the highest enrichment ratio (1.95). A summary of the significantly annotated (FDR corrected) pathways with a focus on neuronal morphogenesis and regulation are presented as a bar diagram showing the enrichment of genes under each term (Fig. 3).

Next, in order to create an integrated visualization network to determine involvement of neuronal morphogenesis, growth and survival factors, a select list of 55 genes from WebGestalt analysis were used in the Metascape program. The enrichment visualization network resulted from the analysis was quite interesting and for the first time show intra- and inter-cluster similarities of enriched terms based on overrepresented gene list. As presented in Fig. 4A, the network was mapped with 20 enriched terms connected by two major domains and three smaller subdoamins. In particular, the terms associated with two major domains in the network were critically enriched (based on calculation using accumulative hypergeometric p-values and enrichment factors) for their roles in regulating phosphatidyl signaling, GTPase signaling, neuron migration and NTRK based neurotrophin signaling. The network is colored by cluster ID, where nodes that share the same cluster IDs are typically close to each other. In Fig. 4B, the same enrichment network has its nodes colored by p-value. The darker the color, the more statistically significant the node is (see legend for p-value ranges). The network result is also presented in a color-coded bar plot in Fig. 4C. Each bar in the plot shows enriched terms across input gene lists, and color coded with respective p-values.

## 4. Discussion

This is the first study to examine transcriptome-wide miRNA expression changes in ACC of MDD subjects using next-generation miRNA sequencing. Based on sequencing results, we detected 2540 annotated miRNAs and 423 novel miRNAs. Of those, 230 miRNAs were significantly altered in MDD subjects compared to control subjects. When directionality of expression was considered, we found that 117 miRNAs (4.61%) were significantly upregulated and 54 (2.13%) were downregulated in MDD subjects (n=22) compared with non-psychiatric controls (n=25). Our web centric parameters and ontology enrichment functions (based on predicted target genes) identified two major domains related to phosphatidyl signaling, GTPase signaling, neuronal migration, and neurotrophin signaling.

In a previous qPCR-based study of 29 miRNAs, Azevedo et al (2016) found decreased expression of miR-34a and miR-184e in ACC of MDD subjects, however, these changes could not survived multiple correction testing (Azevedo et al., 2016). Owing to the repressive nature of miRNAs in regulating target gene expression, we selected top 24 significantly upregulated miRNAs (>2 fold) in ACC of MDD subjects for their possible role in MDD pathogenesis. Our prediction based results helped in finding many target genes that are important in glutamatergic system (GRIN1 and GRIA2) and neurotrophin signaling

(NTRK2 and NTRK3) as well neuronal morphogenesis. The upregulated 24 miRNAs that were used in the prediction analysis were relatively new and their functions have not been extensively characterized. Nevertheless, we conducted gene set enrichment analysis to determine relevant neurobiological functions on the basis of stringent statistical parameters. Intra- and inter-cluster similarities of enriched terms based on overrepresented gene list showed neurobiological functions associated with neuronal growth and survival.

The network enrichment map based on ShinyGO results showed predominance of ontological terms that were correlated with somatic (neuronal cell body), somatodendritic, and presynaptic, postsynaptic, and synaptic vesicle functions. Additionally, we mapped the targeted enrichment of genes translating to glutamatergic synapse which has earlier been shown to play important role in ACC functions associated with MDD pathogenesis. Other reports have previously suggested the role of specific biological factors and their dysregulation in complex behavioral manifestations including MDD and MDD associated suicidal behavior (Pandey, 2013). Several of them have been tested for their prognostic values in predicting complex suicidal behavior (e.g., suicide attempts); however, only a handful of them have proved to be reliable in clinical practices. For instance, the levels of prolactin and thyroid hormone have been found to be associated with suicide attempts in psychiatric patients (Pompili et al., 2012). Moreover, showing the predicted involvement of various other neuro-molecular pathways such as ErbB, Wnt, MAPK, mTOR, and phosphatidylinositol signaling made these findings much more relevant. These pathways have been suggested to play critical roles in maintaining neuronal health and activity under normal conditions but are significantly modified in MDD. We also identified significant enrichment of pathways related to immunomodulatory functions, primarily underlying pro-inflammatory functions mediated through cytokines such as interleukin-17 and tumor necrosis factor (TNF) and their regulatory factors NF-kappa B (NF-kB). This is the first report showing miRNA-mediated regulation of pro-inflammatory genes/pathways in ACC of MDD subjects. This is in line with a previous report showing similar inflammatory activation in ACC by peripheral cytokines where inflammation-associated mood deterioration was significantly correlated with enhanced activity of subgenual anterior cingulate cortex (sACC) (Harrison et al., 2009). NF-kB signaling pathway (NFKB1) is important in MDD pathogenesis from neurotrophin point of view. It has been suggested that the p75NTR, a proBDNF receptor, activates the NF-kB signaling pathway, which results in the alterations of transcription of multiple genes involved to promote neuronal death such as toll-like receptors (TLRs) and tumor necrosis factor-alpha (TNF-α) (Napetschnig and Wu, 2013; Sugiyama et al., 2016). It appears that there is an integrated tripartite relationship between miRNAs, inflammation and neurotrophic activity, which might hold the possibility for deprivation of neuronal growth and functioning in ACC under MDD pathogenesis.

Our results from WebGestalt analysis suggested functional deficits associated with LTP, neurotrophin signaling, and axon guidance. It has earlier been suggested that the postsynaptic form of LTP in the ACC synapse depends on the activation of N-methyl-D-aspartate receptors (NMDARs), a type of glutamate receptor (Li et al., 2017; Zhao et al., 2005). In addition, decreased levels of gamma-aminobutyric acid (GABA) made by glutamate with glutamate decarboxylase (GAD), has also been reported in the ACC of MDD subjects (Price et al., 2009; Schur et al., 2016). Altogether, this shows that in ACC, the LTP

modulation in MDD subjects could be associated with upregulation in certain miRNAs via NMDA receptor dysregulation. On the other, axon guidance is known as a key determinant in the formation of neuronal networks. As mentioned above, miRNA-based prediction results found several target genes that play key roles in axon and dendrite formation (Cariboni et al., 2011; Cobos et al., 2007; Dickson and Gilestro, 2006; Erskine et al., 2011; Mastick et al., 2010). Therefore, our miRNA findings may highlight that MDD associated morphometric deficits in ACC could be due to altered dendritic formation and their connecting networks.

As mentioned in results section, using Metascape program, we prepared enrichment visualization networks. The outcomes were very interesting and showed for the first time intra- and inter-cluster similarities of enriched terms based on overrepresented gene list defining neurobiological functions that either were associated with neuronal growth or survival. With the help of web centric parameters and ontology enrichment functions (based on calculation using accumulative hypergeometric p-values and enrichment factors), we were able to identify two major domains in the network. Interestingly, they built the most cohesive part of the network enrichment with terms associated with phosphatidylinositol signaling, GTPase signaling, neuron migration and most importantly NTRK (receptor for BDNF) based neurotrophin signaling. These results reconfirmed our findings from other two web centric prediction analysis programs (ShinyGo and WebGestalt). This is highly encouraging given that the Metascape analysis is based on 40 independent knowledgebase to integrate system level information and creating a comprehensive gene list. Moreover, the enrichment scores for creating the networks were infringed with rigorous statistical clustering.

Altogether our results identified significant changes in miRNA expression in ACC of MDD subjects. Functional annotation from all three prediction programs consistently highlighted the role miRNAs central to neuronal growth, morphogenesis and differentiation. Precisely, the neuronal atrophy and reduction in volume of ACC, which is hallmark of MDD pathology (Koolschijn et al., 2009), could be considered as potential loss of gene function due to the changes in miRNA landscape. Our comparison with MDD suicide and non-suicide groups suggest that these miRNAs were not specifically associated with suicide as has been reported earlier in dlPFC, where some miRNAs were explicitly related to suicidal behavior (Wang et al., 2018). Interestingly, miRNAs that were altered in ACC of MDD subjects, did not overlap with miRNAs that were dysregulated in other brain areas such as dlPFC (Smalheiser et al., 2012) and locus coeruleus (Roy et al., 2017b). This suggests that specific miRNAs may be regulating gene network(s) or functions that could be critical in ACC functioning and relevant to MDD pathogenesis. In the future, gene expression studies need to be performed to examine precise miRNA functioning in ACC of MDD subjects.

From gene regulation perspective, miRNA acts as repressor of target gene expression, thus large scale miRNA expression profiling can inform systems-level changes in gene regulation. Measurement of the relative abundance of a cohort of miRNAs, ranging from a few significantly altered miRNAs to a group of several miRNAs closely adhered to a specific neurobiological pathway (e.g., phosphatidyl signaling, GTPase signaling and

neurotrophin signaling) could help underpinning the causal association. This may help strengthen strategize precision treatment towards a set of targets.

## Supplementary Material

Refer to Web version on PubMed Central for supplementary material.

## Acknowledgements

This work was supported by the National Institutes of Health (R01MH082802; R01MH101890; R01MH100616; R01MH107183-01; R01MH118884) and American Foundation for Suicide Prevention (SRG-1-042-14) to Dr. Y. Dwivedi.

Role of funding source

Funding agencies had no further role in study design; in the collection, analysis and interpretation of data; in the writing of the report; and in the decision to submit the paper for publication. Research reported in this publication was supported by the National Institute On Alcohol Abuse And Alcoholism of the National Institutes of Health under Award Number R28AA012725. The content is solely the responsibility of the authors and does not necessarily represent the official views of the National Institutes of Health

## References

Azevedo JA, et al., 2016 The microRNA network is altered in anterior cingulate cortex of patients with unipolar and bipolar depression. J Psychiatr Res 82, 58–67. [PubMed: 27468165]

Blackburn TP, 2019 Depressive disorders: Treatment failures and poor prognosis over the last 50 years. Pharmacol Res Perspect 7, e00472. [PubMed: 31065377]

Briggs JA, et al., 2015 Mechanisms of Long Non-coding RNAs in Mammalian Nervous System Development, Plasticity, Disease, and Evolution. Neuron 88, 861–877. [PubMed: 26637795]

Bush G, et al., 2000 Cognitive and emotional influences in anterior cingulate cortex. Trends Cogn Sci 4, 215–222. [PubMed: 10827444]

Cariboni A, et al., 2011 VEGF signalling controls GnRH neuron survival via NRP1 independently of KDR and blood vessels. Development 138, 3723–3733. [PubMed: 21828096]

Cobos I, et al., 2007 Dlx transcription factors promote migration through repression of axon and dendrite growth. Neuron 54, 873–888. [PubMed: 17582329]

Cotter D, et al., 2002 The density and spatial distribution of GABAergic neurons, labelled using calcium binding proteins, in the anterior cingulate cortex in major depressive disorder, bipolar disorder, and schizophrenia. Biol Psychiatry 51, 377–386. [PubMed: 11904132]

Dedova I, et al., 2009 The importance of brain banks for molecular neuropathological research: The New South Wales Tissue Resource Centre experience. Int J Mol Sci 10, 366–384. [PubMed: 19333451]

Dickson BJ, Gilestro GF, 2006 Regulation of commissural axon pathfinding by slit and its Robo receptors. Annu Rev Cell Dev Biol 22, 651–675. [PubMed: 17029581]

Drevets WC, et al., 2008 The subgenual anterior cingulate cortex in mood disorders. CNS spectrums 13, 663–681. [PubMed: 18704022]

Erskine L, et al., 2011 VEGF signaling through neuropilin 1 guides commissural axon crossing at the optic chiasm. Neuron 70, 951–965. [PubMed: 21658587]

Gabbay V, et al., 2012 Anterior cingulate cortex gamma-aminobutyric acid in depressed adolescents: relationship to anhedonia. Arch Gen Psychiatry 69, 139–149. [PubMed: 21969419]

Harrison NA, et al., 2009 Inflammation causes mood changes through alterations in subgenual cingulate activity and mesolimbic connectivity. Biol Psychiatry 66, 407–414. [PubMed: 19423079]

Harrison PJ, et al., 1995 The relative importance of premortem acidosis and postmortem interval for human brain gene expression studies: selective mRNA vulnerability and comparison with their encoded proteins. Neurosci Lett 200, 151–154. [PubMed: 9064599]

Kocerha J, et al., 2015 Noncoding RNAs and neurobehavioral mechanisms in psychiatric disease. Mol Psychiatry 20, 677–684. [PubMed: 25824307]

Koolschijn PC, et al., 2009 Brain volume abnormalities in major depressive disorder: a meta-analysis of magnetic resonance imaging studies. Hum Brain Mapp 30, 3719–3735. [PubMed: 19441021]

Li XH, et al., 2017 Characterization of postsynaptic calcium signals in the pyramidal neurons of anterior cingulate cortex. Mol Pain 13, 1744806917719847. [PubMed: 28726541]

Lim GY, et al., 2018 Prevalence of Depression in the Community from 30 Countries between 1994 and 2014. Sci Rep 8, 2861. [PubMed: 29434331]

Malki K, et al., 2015 Identification of genes and gene pathways associated with major depressive disorder by integrative brain analysis of rat and human prefrontal cortex transcriptomes. Transl Psychiatry 5, e519. [PubMed: 25734512]

Mastick GS, et al., 2010 Longitudinal axons are guided by Slit/Robo signals from the floor plate. Cell Adh Migr 4, 337–341. [PubMed: 20215865]

Napetschnig J, Wu H, 2013 Molecular basis of NF-kappaB signaling. Annu Rev Biophys 42, 443–468. [PubMed: 23495970]

Pandey GN, 2013 Biological basis of suicide and suicidal behavior. Bipolar Disord 15, 524–541. [PubMed: 23773657]

Pizzagalli D, et al., 2001 Anterior cingulate activity as a predictor of degree of treatment response in major depression: evidence from brain electrical tomography analysis. Am J Psychiatry 158, 405–415. [PubMed: 11229981]

Pompili M, et al., 2012 Prolactin and thyroid hormone levels are associated with suicide attempts in psychiatric patients. Psychiatry Res. 200, 389–394. [PubMed: 22748186]

Pompili M, et al., 2013 Bereavement after the suicide of a significant other. Indian J. Psychiatry 55, 256–263. [PubMed: 24082246]

Price RB, et al., 2009 Amino acid neurotransmitters assessed by proton magnetic resonance spectroscopy: relationship to treatment resistance in major depressive disorder. Biol Psychiatry 65, 792–800. [PubMed: 19058788]

Qureshi IA, Mehler MF, 2013 Long non-coding RNAs: novel targets for nervous system disease diagnosis and therapy. Neurotherapeutics 10, 632–646. [PubMed: 23817781]

Radley JJ, et al., 2008 Repeated stress alters dendritic spine morphology in the rat medial prefrontal cortex. J Comp Neurol 507, 1141–1150. [PubMed: 18157834]

Roy B, et al., 2017a Identification of MicroRNA-124–3p as a Putative Epigenetic Signature of Major Depressive Disorder. Neuropsychopharmacology : official publication of the American College of Neuropsychopharmacology 42, 864–875. [PubMed: 27577603]

Roy B, et al., 2017b Altered miRNA expression network in locus coeruleus of depressed suicide subjects. Sci Rep 7, 4387. [PubMed: 28663595]

Salta E, De Strooper B, 2012 Non-coding RNAs with essential roles in neurodegenerative disorders. Lancet Neurol 11, 189–200. [PubMed: 22265214]

Sartor GC, et al., 2012 The Emerging Role of Non-Coding RNAs in Drug Addiction. Front Genet 3, 106. [PubMed: 22737160]

Schmaal L, et al., 2017 Cortical abnormalities in adults and adolescents with major depression based on brain scans from 20 cohorts worldwide in the ENIGMA Major Depressive Disorder Working Group. Mol Psychiatry 22, 900–909. [PubMed: 27137745]

Schur RR, et al., 2016 Brain GABA levels across psychiatric disorders: A systematic literature review and meta-analysis of (1) H-MRS studies. Hum Brain Mapp 37, 3337–3352. [PubMed: 27145016]

Sheedy D, et al., 2008 An Australian Brain Bank: a critical investment with a high return! Cell Tissue Bank 9, 205–216. [PubMed: 18543078]

Smalheiser NR, et al., 2012 MicroRNA expression is down-regulated and reorganized in prefrontal cortex of depressed suicide subjects. PLoS One 7, e33201. [PubMed: 22427989]

Stevens FL, et al., 2011 Anterior cingulate cortex: unique role in cognition and emotion. J Neuropsychiatry Clin Neurosci 23, 121–125. [PubMed: 21677237]

Sugiyama K., et al., 2016 NF-kappaB activation via MyD88-dependent Toll-like receptor signaling is inhibited by trichothecene mycotoxin deoxynivalenol. J Toxicol Sci 41, 273–279. [PubMed: 26961612]

Wang Q, et al., 2018 Role of Complex Epigenetic Switching in Tumor Necrosis Factor-alpha Upregulation in the Prefrontal Cortex of Suicide Subjects. Am J Psychiatry 175, 262–274. [PubMed: 29361849]

Wellman CL, 2001 Dendritic reorganization in pyramidal neurons in medial prefrontal cortex after chronic corticosterone administration. J Neurobiol 49, 245–253. [PubMed: 11745662]

Wise T, et al., 2017 Common and distinct patterns of grey-matter volume alteration in major depression and bipolar disorder: evidence from voxel-based meta-analysis. Mol Psychiatry 22, 1455–1463. [PubMed: 27217146]

Wu H, et al., 2016 Changed Hub and Corresponding Functional Connectivity of Subgenual Anterior Cingulate Cortex in Major Depressive Disorder. Front Neuroanat 10, 120. [PubMed: 28018183]

Zhao MG, et al., 2005 Roles of NMDA NR2B subtype receptor in prefrontal long-term potentiation and contextual fear memory. Neuron 47, 859–872. [PubMed: 16157280]

Zhou Y, et al., 2019 Metascape provides a biologist-oriented resource for the analysis of systems-level datasets. Nat Commun 10, 1523. [PubMed: 30944313]

## Highlights

- Expression levels of miRNAs were determined in anterior cingulate cortex of MDD subjects by miRNA-seq.
- A significant number of miRNAs were differentially regulated in MDD subjects.
- Predicted target-based gene ontology suggested that altered miRNAs may be related to abnormalities in neuronal functions, atrophy and volume loss in ACC of MDD subjects.

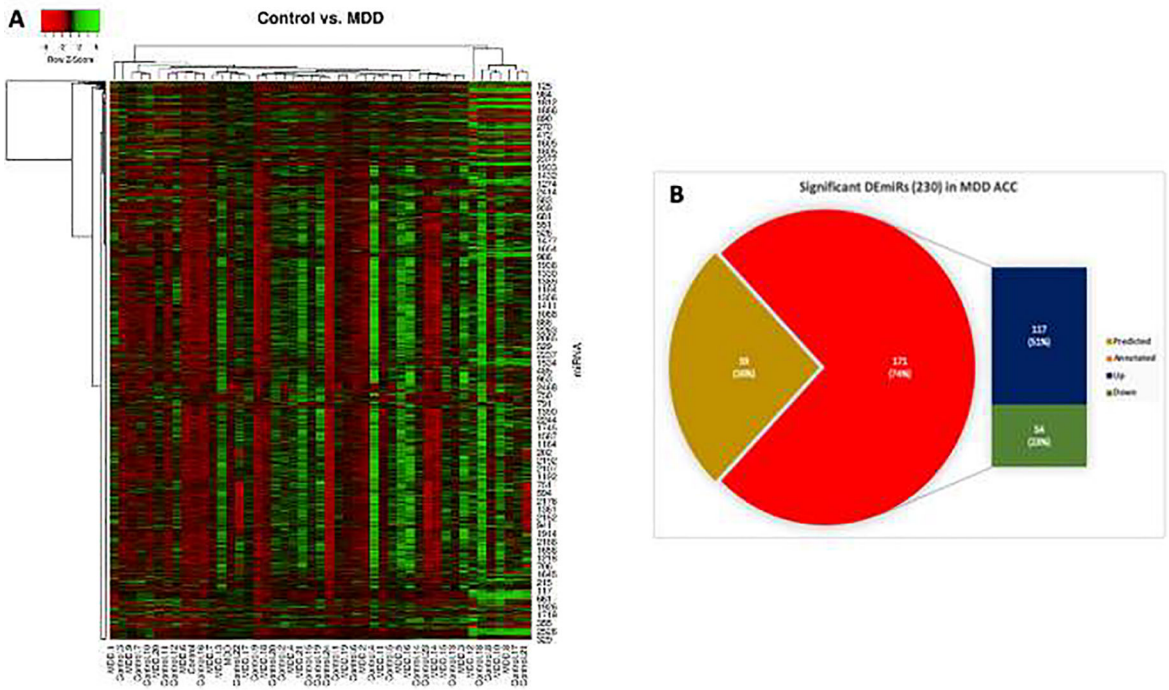


**Fig. 1: miRNA expression heatmap and differentially expressed miRNAs**

A) All 2540 annotated miRNAs and their normalized values between MDD and control (n = 22 vs 25) subjects were plotted in an expression heatmap with hierarchical clustering. Green and red color in the map show higher and lower expression values respectively. For the clustering purposes, the Euclidean method was used to measure the distance, and the average linkage algorithm was applied to calculate the average pairwise distance between all pairs of points. Following the average linkage clustering algorithm, the dendrogram was constructed to demonstrate the expression similarities. B) MDD specific numerical distribution of significantly altered miRNAs was presented with a bar of pie diagram. The pie plot shows the distribution of differentially expressed 171 annotated miRNAs and 59 predicted miRNAs based on their significance level ($p<0.05$). The 117 up and 54 downregulated miRNAs from the list of 171 annotated miRNAs were plotted with a bar diagram.

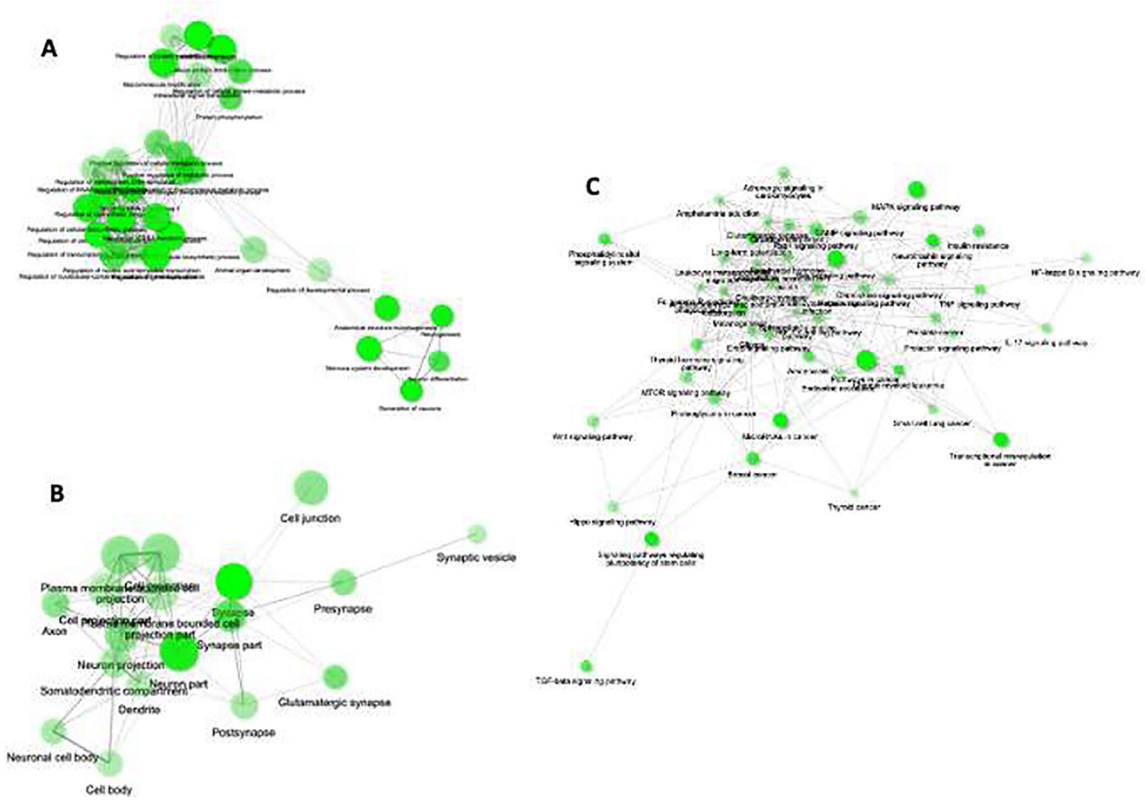


**Fig. 2: Gene ontology and pathway prediction**

GO terms for A) biological process and B) cellular component based on predicted 1,092 target genes. The GO prediction analysis was done following an FDR corrected p-value cutoff 0.05 to determine the gene set enrichment in biological process and cellular component category separately by ShinyGO program. Each category the enriched terms were used to create networks where nodes are presented with terms and connected with edges. As shown in the graphs, if two nodes are connected, then they share 20% (default) or more genes. Bigger nodes represent larger gene sets. Thicker edges represent more overlapped genes. C) A pathway-based network map (p value cutoff <0.05 [FDR], Edge Cutoff: 0.2; most significant display terms: 50) was prepared showing the predicted involvement of various neuro-molecular pathways, those are earlier reported to be important in MDD pathogenesis.

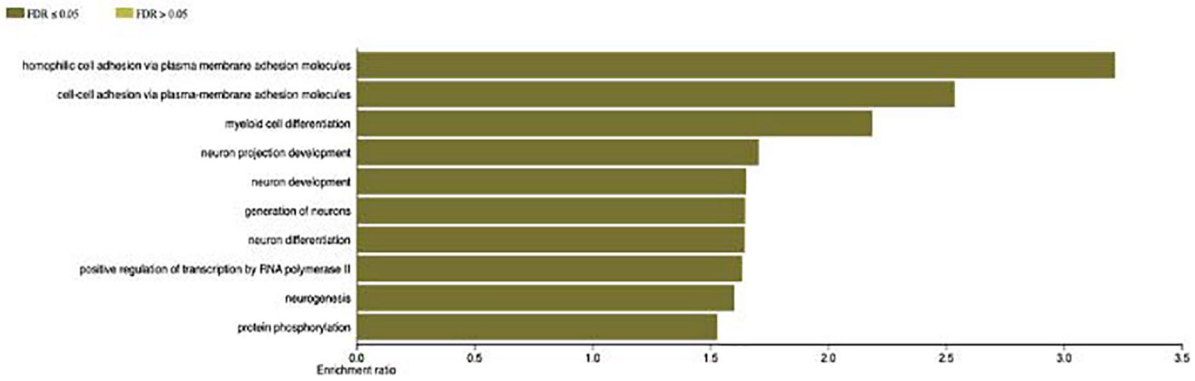


**Fig. 3: Significantly annotated top 10 biological pathway**

GO terms for biological process was predicted by WEB-based GEne SeT AnaLysis Toolkit (WebGestalt, http://www.webgestalt.org/). The significantly annotated (FDR corrected) pathways with a focus on neuronal morphogenesis and regulation are presented as a bar diagram showing the enrichment of genes under each term.

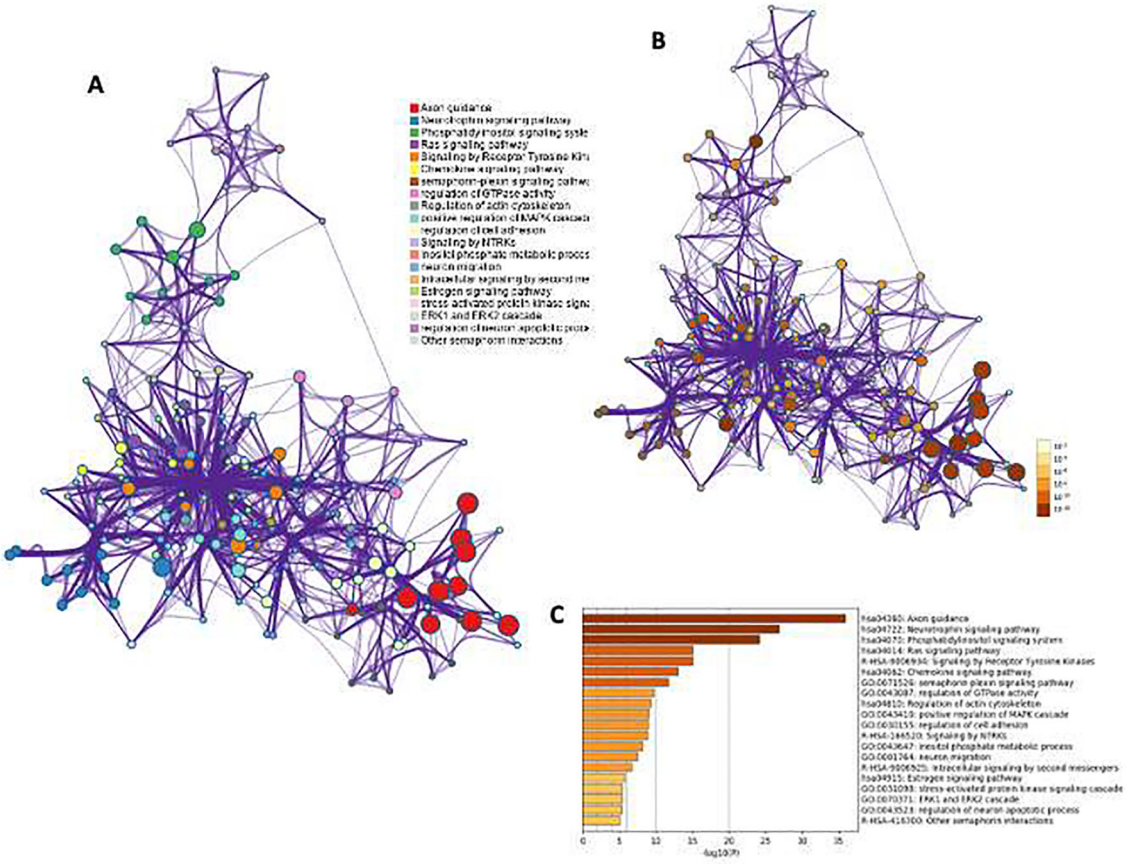


**Fig. 4: The enrichment visualization network based on overrepresented gene list**

A) The network was mapped with 20 enriched terms connected by two major domains and three smaller sub-domains. B) Representation of same enrichment network with colored coded (nodes) p-value. The darker the color, the more statistically significant the node is (see legend for p-value ranges) and C) the same enrichment terms presented listed up as a color-coded bar plot.

**Table 1.**

Demographic and clinical characteristics of control and MDD subjects

| | | Control | MDD | p-value |
|---|---|---|---|---|
| **Number of subjects** | | 25 | 22 | N/A |
| **Age (Year)** | | 50.8 ± 10.6 | 51.6 ± 12.9 | 0.809 |
| **Gender** | **Male** | 15 | 12 | N/A |
| | **Female** | 10 | 10 | |
| **Postmortem interval (Hour)** | | 28.5 ± 15.3 | 29.5 ± 9.7 | 0.781 |
| **Brain pH** | | 6.5 ± 0.4 | 6.6 ± 0.3 | 0.328 |
| **Alcohol abuse** | | 0 | 4 | N/A |
| **Antidepressant drugs** | | 0 | 18 | N/A |
| **Suicide** | | 0 | 10 | N/A |
| **Cause of death** | | Cardiac arrest, respiratory failure | Cardiac arrest, cancer, trauma, hepatic abnormalities, Ischemic bowel | N/A |
| **Method of suicide** | | N/A | Drug toxicity, hanging | |

Values denote mean ± standard deviation. MDD: Major Depressive Disorder, N/A: not applicable.

**Table 2.**

Significantly altered miRNAs in ACC of MDD group (p≥ 0.05)

| miRNA | miRBase ACC No. | Fold change | p-value | Chromosomal location |
|---|---|---|---|---|
| **Up-regulated** | | | | |
| **hsa-miR-6077** | MIMAT0023702 | 2.59 | 1.9E-05 | chr1: 148388282–148388363 [+] |
| **hsa-miR-4632-3p** | MIMAT0019688 | 2.69 | 2.2E-05 | chr1: 12191713–12191773 [+] |
| **hsa-miR-6789-3p** | MIMAT0027479 | 2.49 | 0.00017 | chr19: 2235829–2235926 [−] |
| **hsa-miR-648** | MIMAT0003318 | 2.41 | 0.00025 | chr22: 17980868–17980961 [−] |
| **hsa-miR-4498** | MIMAT0019033 | 2.83 | 0.00049 | chr12: 120155434–120155499 [−] |
| **hsa-miR-6084** | MIMAT0023709 | 2.22 | 0.0007 | chr1: 20633679–20633788 [+] |
| **hsa-miR-4433a-3p** | MIMAT0018949 | 2.15 | 0.00095 | chr2: 64340759–64340839 [+] |
| **hsa-miR-4638-5p** | MIMAT0019695 | 2.04 | 0.00128 | chr5: 181222566–181222633 [−] |
| **hsa-miR-4258** | MIMAT0016879 | 2.39 | 0.00142 | chr1: 154975693–154975783 [+] |
| **hsa-miR-6850-5p** | MIMAT0027600 | 2.01 | 0.00168 | chr8: 144791931–144791991 [−] |
| hsa-miR-4510 | MIMAT0019047 | 1.62 | 0.00171 | chr15: 35926856–35926923 [+] |
| **hsa-miR-3651** | MIMAT0018071 | 2.47 | 0.00173 | chr9: 92292458–92292547 [−] |
| **hsa-miR-4497** | MIMAT0019032 | 2.73 | 0.00243 | chr12: 109833348–109833436 [+] |
| **hsa-miR-668-5p** | MIMAT0026636 | 2.62 | 0.00244 | chr14: 101055258–101055323 [+] |
| hsa-miR-6800-3p | MIMAT0027501 | 1.72 | 0.00291 | chr19: 49832018–49832099 [+] |
| **hsa-miR-7108-3p** | MIMAT0028114 | 2.81 | 0.00474 | chr19: 2434914–2435000 [−] |
| **hsa-miR-4761-3p** | MIMAT0019909 | 2.96 | 0.00478 | chr22: 19963753–19963834 [+] |
| **hsa-miR-4426** | MIMAT0018941 | 2.56 | 0.00509 | chr1: 192716328–192716390 [+] |
| hsa-miR-4720-3p | MIMAT0019834 | 1.93 | 0.00573 | chr16: 81385018–81385093 [+] |
| hsa-miR-4281 | MIMAT0016907 | 1.78 | 0.00656 | chr5: 176629439–176629500 [−] |
| hsa-miR-1273h-3p | MIMAT0030416 | 1.36 | 0.0066 | chr16: 24203116–24203231 [+] |
| hsa-miR-4736 | MIMAT0019862 | 1.84 | 0.00694 | chr17: 58335976–58336022 [−] |
| hsa-miR-3155a | MIMAT0015029 | 1.49 | 0.00736 | chr10: 6152196–6152277 [+] |
| hsa-miR-1227-5p | MIMAT0022941 | 1.81 | 0.00751 | chr19: 2234062–2234149 [−] |
| hsa-miR-6802-5p | MIMAT0027504 | 1.5 | 0.00762 | chr19: 55239912–55239976 [−] |
| **hsa-miR-572** | MIMAT0003237 | 2.21 | 0.00776 | chr4: 11368827–11368921 [+] |
| **hsa-miR-1470** | MIMAT0007348 | 2.5 | 0.00876 | chr19: 15449548–15449608 [+] |
| **hsa-miR-520f-3p** | MIMAT0002830 | 2.11 | 0.01011 | chr19: 53682159–53682245 [+] |
| hsa-miR-92b-3p | MIMAT0003218 | 1.36 | 0.01019 | chr1: 155195177–155195272 [+] |
| hsa-miR-5572 | MIMAT0022260 | 1.68 | 0.01052 | chr15: 80581103–80581239 [+] |
| **hsa-miR-4746-3p** | MIMAT0019881 | 2.18 | 0.01059 | chr19: 4445978–4446048 [+] |
| hsa-miR-550b-2-5p | MIMAT0022737 | 1.99 | 0.01082 | chr7: 30289794–30289890 [−] |
| hsa-miR-518e-5p | MIMAT0005450 | 1.84 | 0.01137 | chr19: 53729838–53729925 [+] |
| hsa-miR-6781-5p | MIMAT0027462 | 1.66 | 0.01184 | chr17: 42823880–42823943 [−] |
| hsa-miR-6890-3p | MIMAT0027681 | 1.91 | 0.01185 | chr3: 49099854–49099914 [−] |
| hsa-miR-760 | MIMAT0004957 | 1.34 | 0.01196 | chr1: 93846832–93846911 [+] |

| miRNA | miRBase ACC No. | Fold change | p-value | Chromosomal location |
|---|---|---|---|---|
| hsa-miR-516a-3p | MIMAT0006778 | 1.75 | 0.01338 | chr19: 53756741–53756830 [+] |
| hsa-miR-4695-5p | MIMAT0019788 | 1.99 | 0.01347 | chr1: 18883202–18883275 [−] |
| hsa-miR-501-3p | MIMAT0004774 | 1.34 | 0.014 | chrX: 50009722–50009805 [+] |
| hsa-miR-1180-5p | MIMAT0026735 | 1.6 | 0.01427 | chr17: 19344506–19344574 [−] |
| hsa-miR-4728-3p | MIMAT0019850 | 1.86 | 0.01456 | chr17: 39726495–39726561 [+] |
| hsa-miR-523-5p | MIMAT0005449 | 1.79 | 0.01576 | chr19: 53698385–53698471 [+] |
| **hsa-miR-1193** | MIMAT0015049 | 2.45 | 0.01676 | chr14: 101030052–101030129 [+] |
| hsa-miR-4318 | MIMAT0016869 | 1.84 | 0.01778 | chr18: 37657135–37657215 [+] |
| hsa-miR-5580-5p | MIMAT0022273 | 1.82 | 0.01786 | chr14: 53948427–53948484 [−] |
| hsa-miR-7112-5p | MIMAT0028121 | 1.75 | 0.01981 | chr8: 144262673–144262737 [−] |
| hsa-miR-6805-3p | MIMAT0027511 | 1.52 | 0.02005 | chr19: 55388181–55388242 [+] |
| hsa-miR-5587-5p | MIMAT0022289 | 1.46 | 0.02055 | chr16: 535316–535368 [+] |
| hsa-miR-6851-5p | MIMAT0027602 | 1.61 | 0.02114 | chr9: 33467869–33467935 [−] |
| hsa-miR-6814-3p | MIMAT0027529 | 1.53 | 0.02122 | chr21: 41746772–41746841 [−] |
| hsa-miR-4663 | MIMAT0019735 | 1.56 | 0.02128 | chr8: 123215788–123215863 [−] |
| **hsa-miR-6075** | MIMAT0023700 | 2.54 | 0.02134 | chr5: 1510762–1510856 [−] |
| hsa-miR-1343-3p | MIMAT0019776 | 1.37 | 0.02178 | chr11: 34941837–34941920 [+] |
| **hsa-miR-6737-5p** | MIMAT0027375 | 2.61 | 0.2188 | chr1: 153962351–153962420 [−] |
| hsa-miR-6879-3p | MIMAT0027659 | 1.52 | 0.0229 | chr11: 65018505–65018570 [+] |
| **hsa-miR-4701-3p** | MIMAT0019799 | 235 | 0.02293 | chr12: 48771975–48772037 [−] |
| hsa-miR-92b-5p | MIMAT0004792 | 1.6 | 0.02334 | chr1: 155195177–155195272 [+] |
| hsa-miR-6753-5p | MIMAT0027406 | 1.7 | 0.02367 | chr11: 68044794–68044957 [+] |
| hsa-miR-4485-5p | MIMAT0032116 | 1.55 | 0.02503 | chr11: 10508270–10508326 [−] |
| hsa-miR-6769b-5p | MIMAT0027620 | 1.65 | 0.02522 | chr1: 206474803–206474864 [+] |
| hsa-miR-519b-3p | MIMAT0002837 | 1.84 | 0.02561 | chr19: 53695213–53695293 [+] |
| hsa-miR-4430 | MIMAT0018945 | 1.66 | 0.02604 | chr2: 33418516–33418564 [+] |
| hsa-miR-6511b-5p | MIMAT0025847 | 1.38 | 0.0264 | chr16: 2106669–2106753 [−] |
| hsa-miR-595 | MIMAT0003263 | 1.72 | 0.02696 | chr7: 158532718–158532813 [−] |
| hsa-miR-3591-5p | | 1.82 | 0.02726 | |
| hsa-miR-6892-5p | MIMAT0027684 | 1.48 | 0.0278 | chr7: 143382686–143382800 [+] |
| hsa-miR-6769a-5p | MIMAT0027438 | 1.66 | 0.02784 | chr16: 4671318–4671390 [+] |
| hsa-miR-6815-3p | MIMAT0027531 | 1.51 | 0.02888 | chr21: 45478266–45478326 [+] |
| hsa-miR-6082 | MIMAT0023707 | 1.6 | 0.02979 | chr4: 171186184–171186292 [+] |
| hsa-miR-4466 | MIMAT0018993 | 1.8 | 0.03022 | chr6: 156779678–156779731 [−] |
| hsa-miR-4758-5p | MIMAT0019903 | 1.56 | 0.0304 | chr20: 62332487–62332557 [−] |
| hsa-miR-622 | MIMAT0003291 | 1.43 | 0.03112 | chr13: 90231182–90231277 [+] |
| hsa-miR-6851-3p | MIMAT0027603 | 1.6 | 0.03117 | chr9: 33467869–33467935 [−] |
| hsa-miR-521 | MIMAT0002854 | 1.6 | 0.03178 | |
| hsa-miR-521-1 | | | | chr19: 53748636–53748722 [+] |

| miRNA | miRBase ACC No. | Fold change | p-value | Chromosomal location |
|---|---|---|---|---|
| hsa-miR-521-2 | | | | chr19: 53716594–53716680 [+] |
| hsa-miR-636 | MIMAT0003306 | 1.73 | 0.03187 | chr17: 76736450–76736548 [−] |
| hsa-let-7c-3p | MIMAT0026472 | 1.12 | 0.03194 | chr21: 16539828–16539911 [+] |
| hsa-miR-6810-3p | MIMAT0027521 | 1.46 | 0.03235 | chr2: 218341911–218341980 [+] |
| hsa-miR-1247-5p | MIMAT0005899 | 1.58 | 0.03266 | chr14: 101560287–101560422 [−] |
| hsa-miR-3648 | MIMAT0018068 | 1.77 | 0.0332 | |
| hsa-mir-3648-1 | | | | chr21: 8208473–8208652 [+] |
| hsa-mir-3648-2 | | | | chr21: 8986999–8987178 [+] |
| hsa-miR-484 | MIMAT0002174 | 1.31 | 0.03341 | chr16: 15643294–15643372 [+] |
| hsa-miR-3621 | MIMAT0018002 | 1.8 | 0.03348 | chr9: 137169186–137169270 [−] |
| hsa-let-7e-5p | MIMAT0000066 | 1.18 | 0.03408 | chr19: 51692786–51692864 [+] |
| hsa-miR-519d-3p | MIMAT0002853 | 1.43 | 0.03453 | chr19: 53713347–53713434 [+] |
| hsa-miR-486-3p | MIMAT0004762 | 1.43 | 0.03481 | chr8: 41660441–41660508 [−] |
| hsa-miR-3189-3p | MIMAT0015071 | 1.48 | 0.03544 | chr19: 18386562–18386634 [+] |
| hsa-miR-5189-5p | MIMAT0021120 | 1.69 | 0.03563 | chr16: 88468918–88469031 [+] |
| hsa-miR-4522 | MIMAT0019060 | 1.44 | 0.03575 | chr17: 27293910–27293996 [−] |
| hsa-miR-302c-5p | MIMAT0000716 | 1.48 | 0.03583 | chr4: 112648363–112648430 [−] |
| hsa-miR-328-3p | MIMAT0000752 | 1.44 | 0.03667 | chr16: 67202321–67202395 [−] |
| hsa-miR-1-5p | MIMAT0031892 | 1.22 | 0.03697 | chr20: 62554306–62554376 [+] |
| hsa-miR-1234-3p | MIMAT0005589 | 1.39 | 0.03734 | chr8: 144400086–144400165 [−] |
| hsa-miR-6826-3p | MIMAT0027553 | 1.4 | 0.03748 | chr3: 129272146–129272243 [+] |
| hsa-miR-378c | MIMAT0016847 | 1.15 | 0.03837 | chr10: 130962588–130962668 [−] |
| hsa-miR-30d-5p | MIMAT0000245 | 1.11 | 0.03859 | chr8: 134804876–134804945 [−] |
| hsa-miR-7156-3p | MIMAT0028223 | 1.32 | 0.03873 | chr1: 77060143–77060202 [+] |
| hsa-miR-519e-5p | MIMAT0002828 | 1.42 | 0.03896 | chr19: 53679940–53680023 [+] |
| hsa-miR-6869-5p | MIMAT0027638 | 1.57 | 0.03987 | chr20: 1392900–1392961 [−] |
| hsa-miR-3689f | MIMAT0019010 | 1.74 | 0.04079 | chr9: 134850742–134850807 [−] |
| hsa-miR-4512 | MIMAT0019049 | 1.55 | 0.04117 | chr15: 66496958–66497034 [−] |
| hsa-miR-6857-5p | MIMAT0027614 | 1.4 | 0.04123 | chrX: 53405673–53405765 [−] |
| hsa-miR-6889-3p | MIMAT0027679 | 1.47 | 0.04153 | chr22: 41252992–41253050 [−] |
| hsa-miR-6131 | MIMAT0024615 | 1.37 | 0.04303 | chr5: 10478037–10478145 [+] |
| hsa-miR-6510-5p | MIMAT0025476 | 1.53 | 0.04315 | chr17: 41517164–41517217 [−] |
| hsa-miR-4505 | MIMAT0019041 | 1.66 | 0.04334 | chr14: 73758747–73758819 [+] |
| hsa-miR-4685-3p | MIMAT0019772 | 1.4 | 0.04387 | chr10: 98431292–98431360 [−] |
| hsa-miR-4530 | MIMAT0019069 | 1.82 | 0.04423 | chr19: 39409623–39409678 [−] |
| hsa-miR-6794-5p | MIMAT0027488 | 1.56 | 0.04427 | chr19: 12852260–12852327 [+] |
| hsa-miR-125b-2-3p | MIMAT0004603 | 1.17 | 0.04465 | chr21: 16590237–16590325 [+] |
| hsa-miR-4538 | MIMAT0019081 | 1.54 | 0.04479 | chr14: 105858165–105858242 [−] |
| hsa-miR-663b | MIMAT0005867 | 1.8 | 0.0453 | chr2: 132256966–132257080 [−] |

| miRNA | miRBase ACC No. | Fold change | p-value | Chromosomal location |
|---|---|---|---|---|
| hsa-miR-3609 | MIMAT0017986 | 1.42 | 0.04669 | chr7: 98881650–98881729 [+] |
| hsa-miR-2861 | MIMAT0013802 | 1.76 | 0.04701 | chr9: 127785918–127786007 [+] |
| hsa-miR-4783-5p | MIMAT0019946 | 1.4 | 0.04721 | chr2: 127423537–127423618 [−] |
| hsa-miR-671-3p | MIMAT0004819 | 1.26 | 0.04791 | chr7: 151238421–151238538 [+] |
| hsa-miR-3928-5p | MIMAT0027037 | 1.19 | 0.04812 | chr22: 31160062–31160119 [−] |
| hsa-miR-6821-5p | MIMAT0027542 | 1.61 | 0.04932 | chr22: 49962866–49962939 [+] |
| hsa-miR-6853-3p | MIMAT0027607 | 1.24 | 0.0499 | chr9: 35732922–35732995 [+] |
| | | | | |
| **Downregulated** | | | | |
| hsa-miR-136-5p | MIMAT0000448 | 0.73 | 0.00047 | chr14: 100884702–100884783 [+] |
| hsa-miR-551b-3p | MIMAT0003233 | 0.73 | 0.00117 | chr3: 168551854–168551949 [+] |
| **hsa-miR-367-3p** | MIMAT0000719 | 0.45 | 0.00137 | chr4: 112647874–112647941 [−] |
| **hsa-miR-5590-5p** | MIMAT0022299 | 0.46 | 0.00221 | chr2: 134857820–134857873 [+] |
| hsa-miR-337-5p | MIMAT0004695 | 0.84 | 0.00244 | chr14: 100874493–100874585 [+] |
| hsa-miR-1251-5p | MIMAT0005903 | 0.81 | 0.00248 | chr12: 97491909–97491978 [+] |
| hsa-miR-543 | MIMAT0004954 | 0.83 | 0.00361 | chr14: 101031987–101032064 [+] |
| hsa-miR-138-5p | MIMAT0000430 | 0.8 | 0.00399 | chr16: 56858518–56858601 [+] |
| **hsa-miR-20b-3p** | MIMAT0004752 | 0.47 | 0.00427 | chrX: 134169809–134169877 [−] |
| hsa-miR-495-5p | MIMAT0022924 | 0.85 | 0.00475 | chr14: 101033755–101033836 [+] |
| hsa-miR-6808-3p | MIMAT0027517 | 0.62 | 0.00586 | chr1: 1339650–1339708 [−] |
| hsa-miR-4705 | MIMAT0019805 | 0.88 | 0.00765 | chr13: 102045934–102046004 [−] |
| hsa-miR-376a-3p | MIMAT0000729 | 0.81 | 0.00766 | chr14: 101040782–101040849 [+] |
| hsa-miR-4796-3p | MIMAT0019971 | 0.73 | 0.00775 | chr3: 114743445–114743525 [−] |
| hsa-miR-495-3p | MIMAT0002817 | 0.75 | 0.01027 | chr14: 101033755–101033836 [+] |
| hsa-miR-154-5p | MIMAT0000452 | 0.84 | 0.01082 | chr14: 101059755–101059838 [+] |
| hsa-miR-496 | MIMAT0002818 | 0.84 | 0.01097 | chr14: 101060573–101060674 [+] |
| **hsa-miR-548ar-3p** | MIMAT0022266 | 0.46 | 0.01173 | chr13: 114244505–114244561 [+] |
| hsa-miR-670-3p | MIMAT0026640 | 0.75 | 0.01195 | chr11: 43559656–43559753 [+] |
| hsa-miR-488-3p | MIMAT0004763 | 0.85 | 0.01201 | chr1: 177029363–177029445 [−] |
| hsa-miR-29b-2-5p | MIMAT0004515 | 0.9 | 0.01285 | chr1: 207802443–207802523 [−] |
| hsa-miR-497-5p | MIMAT0002820 | 0.86 | 0.01297 | chr17: 7017911–7018022 [−] |
| hsa-miR-335-5p | MIMAT0000765 | 0.87 | 0.01304 | chr7: 130496111–130496204 [+] |
| hsa-miR-487a-3p | MIMAT0002178 | 0.82 | 0.01611 | chr14: 101052446–101052525 [+] |
| hsa-miR-544a | MIMAT0003164 | 0.8 | 0.01635 | chr14: 101048658–101048748 [+] |
| hsa-miR-342-5p | MIMAT0004694 | 0.89 | 0.01789 | chr14: 100109655–100109753 [+] |
| hsa-miR-1197 | MIMAT0005955 | 0.82 | 0.01812 | chr14: 101025564–101025651 [+] |
| hsa-miR-153-5p | MIMAT0026480 | 0.81 | 0.01966 | chr7: 157574336–157574422 [−] |
| hsa-miR-6844 | MIMAT0027589 | 0.78 | 0.0209 | chr8: 124508515–124508576 [−] |
| hsa-miR-758-3p | MIMAT0003879 | 0.85 | 0.02115 | chr14: 101026020–101026107 [+] |
| hsa-miR-22-5p | MIMAT0004495 | 0.87 | 0.02205 | chr17: 1713903–1713987 [−] |

| miRNA | miRBase ACC No. | Fold change | p-value | Chromosomal location |
|---|---|---|---|---|
| hsa-miR-29b-3p | MIMAT0000100 | 0.85 | 0.02327 | chr7: 130877459–130877539 [−] |
| hsa-miR-377-3p | MIMAT0000730 | 0.83 | 0.02501 | chr14: 101062050–101062118 [+] |
| hsa-miR-153-3p | MIMAT0000439 | 0.8 | 0.02614 | chr2: 219294111–219294200 [−] |
| hsa-miR-2277-5p | MIMAT0017352 | 0.9 | 0.02674 | chr5: 93620696–93620788 [−] |
| hsa-miR-9-3p | MIMAT0000442 | 0.9 | 0.02713 | chr1: 156420341–156420429 [−] |
| hsa-miR-1307-5p | MIMAT0022727 | 0.83 | 0.03086 | chr10: 103394253–103394401 [−] |
| hsa-miR-548a-3p | MIMAT0003251 | 0.72 | 0.03186 | chr6: 18571784–18571880 [+] |
| hsa-miR-494-3p | MIMAT0002816 | 0.9 | 0.03362 | chr14: 101029634–101029714 [+] |
| hsa-miR-22-3p | MIMAT0000077 | 0.89 | 0.03656 | chr17: 1713903–1713987 [−] |
| **hsa-miR-3689a-5p** | MIMAT0018117 | 0.43 | 0.03897 | chr9: 134849487–134849564 [−] |
| hsa-miR-146a-5p | MIMAT0000449 | 0.9 | 0.04076 | chr5: 160485352–160485450 [+] |
| hsa-miR-4477b | MIMAT0019005 | 0.81 | 0.04126 | chr9: 41233755–41233835 [−], chr9: 63819574–63819654 [+] |
| hsa-miR-582-3p | MIMAT0004797 | 0.88 | 0.04397 | chr5: 59703606–59703703 [−] |
| hsa-miR-7-1-3p | MIMAT0004553 | 0.9 | 0.04513 | chr9: 83969748–83969857 [−] |
| hsa-miR-376c-3p | MIMAT0000720 | 0.83 | 0.04613 | chr14: 101039690–101039755 [+] |
| hsa-miR-135b-5p | MIMAT0000758 | 0.85 | 0.04615 | chr1: 205448302–205448398 [−] |
| hsa-miR-376a-5p | MIMAT0003386 | 0.86 | 0.04712 | chr14: 101040782–101040849 [+] |
| hsa-miR-128-2-5p | MIMAT0031095 | 0.62 | 0.04776 | chr3: 35744476–35744559 [+] |
| hsa-miR-376c-5p | MIMAT0022861 | 0.85 | 0.04836 | chr14: 101039690–101039755 [+] |
| hsa-miR-5582-3p | MIMAT0022280 | 0.63 | 0.04923 | chr11: 46753125–46753192 [−] |
| hsa-miR-548ac | MIMAT0018938 | 0.53 | 0.04978 | chr1: 116560024–116560111 [−] |
| hsa-miR-3182 | MIMAT0015062 | 0.7 | 0.04988 | chr16: 83508346–83508408 [+] |
| hsa-miR-548a-5p | MIMAT0004803 | 0.72 | 0.04997 | chr8: 104484369–104484465 [−] |

Bold face letter miRNAs show fold change >2.0 (upregulated) or <0.5 (downregulated)

**Table 3.**

KEGG pathway results from extremely upregulated 24 miRNAs (fold change cut off >2.0)

| Gene Set | Description | Enrichment ratio | p-value | FDR | Candidate genes |
|---|---|---|---|---|---|
| hsa04720 | Long-term potentiation | 3.4039 | 0.00016382 | 0.0055154 | ADCY1, CALM1, GRIA2, GRIN1, MAPK1, PPP1CB, PRKCA, PRKCB, PRKCG, RAP1A, RPS6KA1, RPS6KA3 |
| hsa05220 | Chronic myeloid leukemia | 3.2509 | 0.00014340 | 0.0055154 | CBL, CDKN1B, GAB2, GADD45A, HDAC2, MAPK1, MYC, NFKB1, NFKBIA, PIK3CD, POLK, RELA, SHC4 |
| hsa04550 | Signaling pathways regulating pluripotency of stem cells | 2.7345 | 0.000035245 | 0.0041494 | ACVR1B, ACVR2B, BMPR1A, FGFR2, FZD10, FZD3, FZD5, IGF1, IL6ST, KAT6A, MAPK1, MEIS1, MYC, ONECUT1, OTX1, PCGF5, PIK3CD, SMAD9, WNT3A, ZFHX3 |
| hsa04722 | Neurotrophin signaling pathway | 2.7150 | 0.00014818 | 0.0055154 | ARHGDIA, CALM1, IRAK2, IRAK4, MAPK1, NFKB1, NFKBIA, NTRK2, NTRK3, PIK3CD, RAN1A, RELA, RPS6KA1, RPS6KA3, RPS6KA5, SHC4, TP73 |
| hsa04360 | Axon guidance | 2.4978 | 0.000040804 | 0.0041494 | ARHGEF12, CFL2, CXCL12, DPYSL5, FZD3, GNAI2, MAPK1, NRP1, PAK2, PAK3, PARD6G, PIK3CD, PLXNA1, PLXNC1, PRKCA, RASA1, ROBO2, ROCK1, SEMA3A, SEMA3C, SEMA5A, SRGAP2, SRGAP3 |
| hsa04014 | Ras signaling pathway | 2.3756 | 0.000010929 | 0.0035628 | ARF6, CALM1, CSF1, FGF1, FGFR2, GAB2, GNGT2, GRIN1, IGF1, KIT, KSR2, MAPK1, NFKB1, NTRK2, PAK2, PAK3, PIK3CD, PRKCA, PRKCB, PRKCG, RAB5B, RAP1A, RASAL2, RASGRF2, RELA, SHC4, STK4, TEK |
| hsa05202 | Transcriptional misregulation in cancer | 2.3501 | 0.00010641 | 0.0055154 | AFF1, CDKN1B, FOXO1, GADD45A, H3F3B, HDAC2, HMGA2, IGF1, IL2RB, KLF3, MEF2C, MEIS1, MMP3, MPO, MYC |
| hsa04144 | Endocytosis | 2.1030 | 0.00018487 | 0.0055154 | AGAP1, ARF6, ARFGEF1, CAPZA1, CBL, CHMP4C, CHMP7, CYTH4, FGFR2, IL2RB, IQSEC2, KIF5C, NEDD4, PARD6G, PIP5K1C, PML, PRKCI, RAB10, RAB11FIP4, RAB31, RAB35, RAB5B, RABEP1, SH3GLB1, SMURF1, SNX12, STAM2 |
| hsa04010 | MAPK signaling pathway | 1.9971 | 0.00016207 | 0.0055154 | CACNA1E, CACNB4, CSF1, DUSP16, FGF1, FGFR2, CADD45A, IGF1, IRAK4, KIT, MAPK1, MEF2C, MKNK2, MYC, NFKB1, NLK, NTRK2, PAK2, PRKCA, PRKCB, PRKCG, RAP1A, RASA1, RASGRF2, RELA, RPS6KA1, RPS6KA3, RPS6KA5, STK4, TAOK1, TEK |
| hsa05200 | Pathways in cancer | 1.7704 | 0.000050912 | 0.0041494 | ADCY1, ADCY2, ARHGEF12, ARNT, CALM1, CBL, CCDC6, CDKN1B, COL4A2, CXCL12, DLL4, EDNRB, ESR1, FGF1, FGFR2, FOXO1, FZD10, FZD3, FZD5, GADD45Am GNAI2, GNGT2, HDAC2, HEY2, IGF1, IL2RB, IL6ST, ITGA2, KIT, LAMC3, MAPK1, MYC, NFKB1, NFKBIA, NOTCH2, PIK3CD, PML, POLK, PRKCA, PRLCB, PRKCG, RELA, ROCK1, RPS6KA5, SP1, STK4, TPM3, TRAF4, WNT3A |

**Table 4.**

Gene ontology results from extremely upregulated 24 miRNAs (fold change cut off >2.0)

| Gene Set | Description | Enrichment ratio | p-value | FDR |
|---|---|---|---|---|
| **Biological Processes (BP)** | | | | |
| GO:0007156 | Homophilic cell adhesion via plasma | 3.2174 | 1.1770e-8 | 0.000035666 |
| GO:0098742 | Cell-cell adhesion via plasma-membrane | 2.5358 | 1.1691e-7 | 0.00017713 |
| GO:0030099 | Myeloid cell differentiation | 2.1868 | 4.9157e-7 | 0.00044689 |
| GO:0031175 | Neuron projection development | 1.7059 | 4.3918e-7 | 0.00044689 |
| GO:0048666 | Neuron development | 1.6533 | 4.7477e-7 | 0.00044689 |
| GO:0048699 | Generation of neurons | 1.6481 | 3.8315e-9 | 0.000034832 |
| GO:0030182 | Neuron differentiation | 1.6467 | 2.6161e-8 | 0.000047566 |
| GO:0045944 | Positive regulation of transcription by RNA | 1.6351 | 2.6580e-7 | 0.00034519 |
| GO:0022008 | Neurogenesis | 1.6031 | 1.0945e-8 | 0.000035666 |
| GO:0006468 | Protein phosphorylation | 1.5305 | 1.9251e-8 | 0.000043753 |
| **Cellular Components (CC)** | | | | |
| GO:0045202 | Synapse | 2.2821 | 0 | 0 |
| GO:0044456 | Synapse part | 2.1256 | 3.8531e- | 8.6364e-9 |
| GO:0030054 | Cell junction | 1.8931 | 1.8015e- | 3.0239e-8 |
| GO:0097458 | Neuron part | 1.8893 | 1.0347e- | 6.0790e-11 |
| GO:0043005 | Neuron projection | 1.8638 | 4.3436e- | 6.3796e-8 |
| GO:0098805 | Whole membrane | 1.8445 | 3.5398e- | 1.3864e-9 |
| GO:0005887 | Integral component of plasma membrane | 1.8253 | 1.6646e- | 4.8899e-9 |
| GO:0031226 | Intrinsic component of plasma membrane | 1.7831 | 4.4101e- | 8.6364e-9 |
| GO:0044463 | Cell projection part | 1.7663 | 3.2440e-9 | 3.8118e-7 |
| GO:0120038 | Plasma membrane bounded cell projection | 1.7663 | 3.2440e-9 | 3.8118e-7 |
| **Molecular Functions (MF)** | | | | |
| GO:0001012 | RNA polymerase II regulatory region | 1.9494 | 2.4542e- | 0.0000094567 |
| GO:0000977 | RNA polymerase II regulatory region | 1.9123 | 8.2815e- | 0.000022206 |
| GO:0016773 | Phosphotransferase activity, alcohol | 1.9041 | 3.4398e- | 0.000010761 |
| GO:0044212 | Transcription regulatory region DNA | 1.8801 | 7.5765e- | 0.0000068572 |
| GO:0001067 | Regulatory region nucleic acid binding | 1.8759 | 8.4200e- | 0.0000068572 |
| GO:0000976 | Transcription regulatory region sequence- | 1.8594 | 1.3786e- | 0.000028751 |
| GO:1990837 | Sequence-specific double-stranded DNA | 1.8351 | 1.3181e- | 0.000028751 |
| GO:0003690 | Double-stranded DNA binding | 1.7775 | 1.6863e- | 0.000031653 |
| GO:0000981 | DNA-binding transcription factor activity, | 1.6004 | 2.5191e- | 0.0000094567 |
| GO:0003700 | RNA -binding transcription factor activity | 1.5945 | 1.0960e- | 0.0000068572 |